JOURNAL OF SPACECRAFT AND ROCKETS
Vol. 45, No. 4, July–August 2008

Erratum

Performance of a Low Density Ablative Heat Shield Material

M. A. Covington* and J. M. Heinemann†
Eloret Corporation, Sunnyvale, California 94086
H. E. Goldstein‡
Research Institute for Advanced Computer Science, Moffett Field, California 94035
and
Y.-K. Chen,§ I. Terrazas-Salinas,‖ J. A. Balboni,¶ J. Olejniczak,** and E. R. Martinez††
NASA Ames Research Center, Moffett Field, California 94035

[*J. Spacecraft*, 45(2), pp. 237–247, (2008)]

DOI: 10.2514/1.38249

Because of a printer error, certain numbers and symbols were missing from the print version of this article, first published in the March–April 2008 issue of the *Journal of Spacecraft and Rockets*. The corrected article is reproduced below in its entirety. AIAA regrets the error.

An evaluation of the Stardust spacecraft forebody heat shield design was conducted to address uncertainties in original development and qualification efforts. Results are reported for additional arc jet tests and analyses done on the ablative and thermal performance of the low density ablative material used in the Stardust design for conditions simulating nominal peak convective heating conditions expected for Stardust sample return capsule Earth entry. Test data were used to adjust iteratively the thermophysical properties in an ablative response computer code to match experimental in-depth temperatures. Ablative recession rates and maximum internal temperatures were satisfactorily predicted by the computer code using derived properties for nominal peak entry heating rates and for rates 37% greater than nominal. Experimental and computer model maximum internal material temperatures were in agreement over a range of conditions and are considered to validate the Stardust heat shield design although measured in-depth temperature data show consistent temperature rise deviations that are not accurately modeled by the computer code. Predicted Stardust heat shield performance based on these results indicates that maximum attachment bond line temperatures will be considerably less than the maximum allowable of 250°C, and total recession will be a small fraction of the as-designed thickness.

I. Introduction

THE renewed interest in space missions to explore other planets has created a need for new advanced heat shield materials capable of efficiently protecting spacecraft under very high heating conditions. Such conditions may be experienced both during entry into the atmospheres of planets of interest and during reentry into Earth's atmosphere for return missions. Very little development of new, efficient ablative materials has been pursued in the past two decades (since the Apollo and Viking spacecraft) due partly to the lack of missions requiring such materials.

The Stardust mission, as part of NASA's Discovery Program in 1995, created a requirement for new ablative heat shields as an enabling technology to meet the spacecraft mass goals. The Stardust mission [1] was designed as a mission to fly by a comet, Wild 2, at close range for the collection of cometary debris as well as to obtain interplanetary dust samples and return them to Earth within a sample return capsule (SRC). The success of the mission requires that this sample return capsule protect the collected samples during Earth atmospheric entry at an inertial velocity of 12.6 km/s by keeping the SRC internal structure at temperatures that meet a science requirement to keep the sample materials below 70°C. These conditions result in nominal values for maximum stagnation point heating flux of 1200 W/cm^2, peak surface pressure of 0.5 atm, and an integrated heat load of 36.5 kJ/cm^2 for the baseline entry.

To meet the requirements for the Stardust mission, one of a family of lightweight ceramic ablator materials developed at NASA Ames Research Center was selected for the forebody heat shield of the Stardust sample return capsule. This material, phenolic impregnated carbon ablator (PICA), consists of a commercially available low density carbon fiber matrix substrate impregnated with phenolic resin. Some characteristics of this family of lightweight ablator materials and processing methods are given in [2].

The Stardust program resulted in intensive material development, modeling, and testing efforts [3] to provide a heat shield for the high

Presented as Paper 2273 at the 37th AIAA Thermophysics Conference, Portland, Oregon, 28 June–1 July 2004; received 3 August 2004; revision received 30 November 2005; accepted for publication 22 December 2005.

*Senior Consultant, 465 South Mathilda Avenue, Suite 103. Senior Member AIAA.
†Research Engineer, 465 South Mathilda Avenue, Suite 103.
‡Senior Consultant. Fellow AIAA.
§Aerospace Engineer.
‖Aerospace Engineer.
¶Research Engineer.
**Senior Research Scientist. Senior Member AIAA.
††Senior Research Engineer.

convective heating conditions expected during Earth entry while under constraints of limited time and funding. Because of uncertainties in the heating rate calibrations carried out under the original test activities, a second project was initiated to reexamine the arc jet test conditions, the PICA ablative and thermal performance, and the modeling used to design the Stardust flight heat shield. Summarized results of this project are presented in this paper.

II. Material Tests and Analyses

A. PICA Material Description

The material used for the Stardust forebody heat shield is one of a class of low density, charring ablative materials recently developed at the NASA Ames Research Center. The PICA material is made from a fibrous carbon matrix insulation (Fiber Materials, Inc., under the trade name Fiberform) impregnated with a commercial phenolic resin. The phenol-formaldehyde resin (SC1008) used in the Stardust formulation creates a porous thermoset material after polymerization that has final bulk densities ranging from 0.22 to 0.27 g/cm^3, depending on the processing employed. More extensive details of PICA materials processing are given in [2].

B. Arc Jet Tests

The tests and related analyses were carried out to investigate the performance of PICA under conditions appropriate to the Stardust entry environment. The program used tests in a high-energy arc jet to obtain needed data on both the ablative performance and the thermal performance of PICA material by varying the model size and the arc jet operating conditions.

The NASA Ames 60 MW Interaction Heating Facility [4] was used to provide the aerothermal test environment required to simulate Stardust SRC entry conditions as it was for the earlier Stardust development and qualification testing. Sixteen PICA flat-faced cylindrical models of 2.54 and 5.08 cm diam were tested to obtain ablative performance data at the approximate conditions expected at the SRC peak convective heating flux and for heating rates at a required heat shield design margin above this. To measure thermal performance, sixteen flat-faced cylindrical models of 10.16 cm diam were tested at lower convective heating rate conditions. Radiation heating from the entry shock layer previously had been found to be unimportant for the Stardust mission [5] as was the case for these arc jet tests. A summary of the configurations of these models and test conditions are given in Tables 1 and 2. The stream enthalpy values in Tables 1 and 2 were deduced from laminar flow heat transfer relationships [6] using the measured pitot pressure and stagnation point heat flux to copper heat sink calorimeters and water-cooled Gardon-type calorimeters.

Experimental test data were compared with computed response results to develop and refine an analytical model that would satisfactorily predict both the ablative and thermal performance of PICA heat shields. These comparisons and results for the prediction of Stardust entry performance are given in more detail in following sections.

1. Test Models

Drawings of the PICA material model configurations are shown in Figs. 1 and 2. The 2.54 and the 5.08 cm diam models are illustrated in Figs. 1a and 1b, respectively, and the 10.16 cm diam models are

Table 1 2.54 and 5.08 cm diam PICA model characteristics and test conditions (IHF 121-I test series)

Model diameter, cm	Model no.	Run no.	Heating time, s	Heating rate, W/cm^2	Total heat load, kJ/cm^2	Stagnation pressure, atm	Enthalpy, MJ/kg	PICA thickness, cm
2.54	22	12W	8	1630	13.0	0.65	29.5	5.72
2.54	23	12E	13	1630	21.2	0.65	29.5	5.72
2.54	24	14W	8	1630	13.0	0.65	29.5	5.72
2.54	26	14E	18	1630	29.3	0.65	29.5	5.72
2.54	27	15W	4	1630	6.5	0.65	29.5	5.72
2.54	28	15E	13	1630	21.2	0.65	29.5	5.72
2.54	29	16W	15	1630	24.5	0.65	29.5	5.72
2.54	30	16E	20	1630	32.6	0.65	29.5	5.72
5.08	10	9E	28	1150	32.2	0.65	29.5	5.66
5.08	11	9W	18	1150	20.7	0.65	29.5	5.66
5.08	12	10E	33	1150	38.0	0.65	29.5	5.66
5.08	13	10W	23	1150	26.5	0.65	29.5	5.66
5.08	15	11E	38	1150	43.7	0.65	29.5	5.66
5.08	14	11W	18	1150	20.7	0.65	29.5	5.66
5.08	17	17E	28	1150	32.2	0.65	29.5	5.66
5.08	16	17W	35	1150	40.2	0.65	29.5	5.66

Table 2 10.16 cm diam PICA model characteristics and test conditions (IHF 121-II test series)

Model diameter, cm	Model no.	Run no.	Heating time, s	Heating rate, W/cm^2	Total heat load, kJ/cm^2	Stagnation pressure, atm	Enthalpy, MJ/kg	PICA thickness, cm
10.16	1	15E	69	580	40.0	0.45	29.5	6.05
10.16	2	15W	86	580	49.9	0.45	29.5	6.05
10.16	3A	14E	20	580	11.6	0.45	29.5	2.23
10.16	3B	13E	40	580	23.2	0.45	29.5	3.25
10.16	4B	13W	20	580	11.6	0.45	29.5	3.25
10.16	6A	14W	20	580	11.6	0.45	29.5	2.23
10.16	7A	12E	15	580	8.7	0.45	29.5	2.74
10.16	7B	12W	15	580	8.7	0.45	29.5	2.74
10.16	8A	11E	10	580	5.8	0.45	29.5	2.74
10.16	8B	11W	20	580	11.6	0.45	29.5	2.74
10.16	4A	17W	30	400	12.0	0.20	29.5	2.23
10.16	5A	17E	30	400	12.0	0.20	29.5	2.23
10.16	5B	18E	40	400	16.0	0.20	29.5	3.25
10.16	6B	18W	60	400	24.0	0.20	29.5	3.25
10.16	9A	16E	15	400	6.0	0.20	29.5	2.74
10.16	9B	16W	29	400	11.6	0.20	29.5	2.74

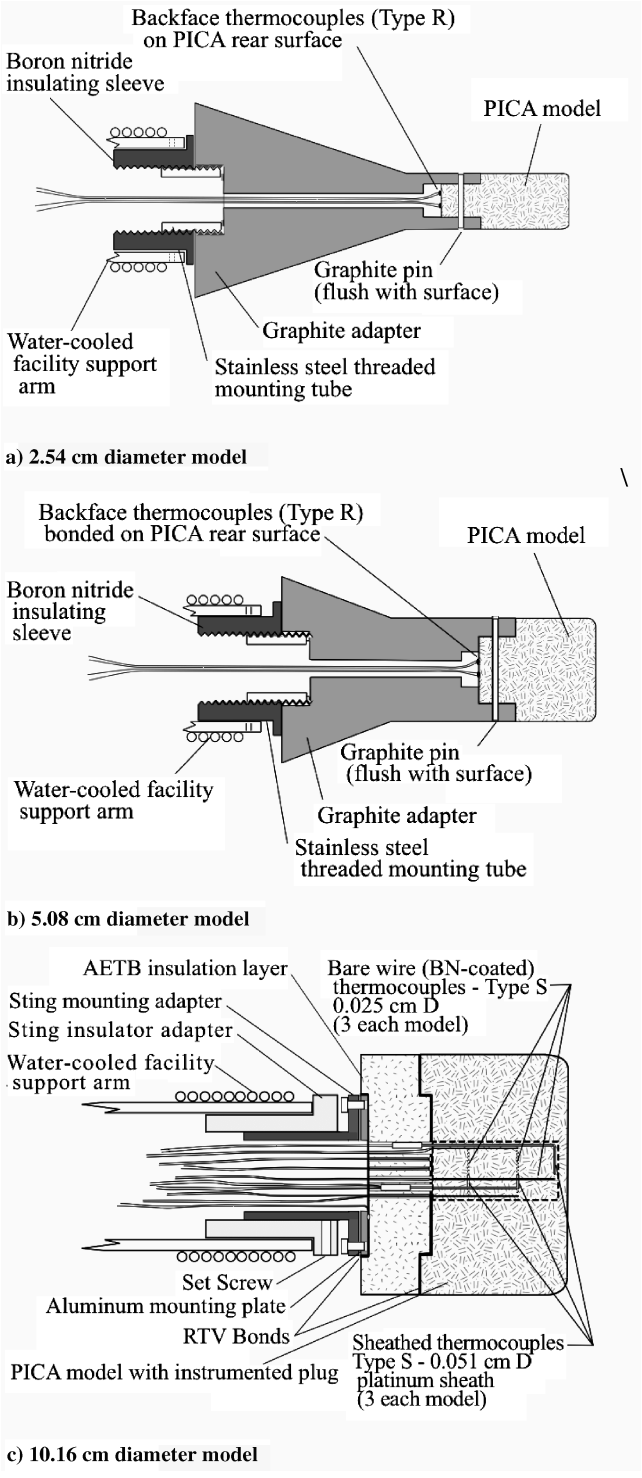

Fig. 1 Assembled PICA models (not to scale).

illustrated in Fig. 1c. Details of the assembled and instrumented 10.16 cm models are shown in Figs. 2a and 2b. The flat-faced 2.54 and 5.08 cm models had a corner radius of 0.239 and 0.476 cm, respectively. The 10.16 cm diam model had a corner radius of 0.953 cm. All models were fabricated from flight-qualified PICA material from the same processing lot as that used for the Stardust flight heat shield. The average density of the PICA billet used for the models was 0.266 g/cm^3 as determined from small samples taken from multiple locations throughout the billet. The sidewalls of 3.54 and 5.08 cm models were uncoated but nearly all of the 10.16 cm models were coated with a graphite-based slurry (Graphi-Bond) to minimize the escape of internally generated pyrolysis gases out the sides.

The 2.54 and 5.08 cm models were retained in a graphite adapter using a graphite pin as shown in Figs. 1a and 1b. These graphite adapters were, in turn, attached to a facility model support arm with a threaded stainless steel mounting tube and a boron nitride insulation sleeve. This insulating sleeve was required to electrically isolate the model from the grounded support arm and reduce noise on the instrumentation signals.

The 10.16 cm diam models were constructed as shown in Fig. 1c with a 2.54 cm thick layer of alumina enhanced thermal barrier (AETB) material behind the PICA layer for thermal isolation and approximation of an adiabatic back wall condition. The PICA samples, AETB layers, and aluminum mounting plates were attached to each other with silicone adhesive as shown in Fig. 1c.

2. *Test Model Instrumentation*

The high heating rates and resulting high material temperatures used in the arc jet tests resulted in limitations on the type and number of material performance measurement sensors that could be incorporated. Because of the high rate of temperature increase and the high maximum temperatures (>3000°C) expected in the 2.54 and 5.08 cm diam models, only backface temperature and surface temperature measurements were made on these models. Backface temperatures were obtained using 0.254 mm diam type R thermocouples attached to the model rear face with a graphite-based cement (Graphi-Bond) as illustrated in Figs. 1a and 1b. Two of these backface thermocouples were attached to each model for redundancy.

The 10.16 cm diam models were instrumented using multiple thermocouple probes and bare wire thermocouples to measure in-depth, bondline, and backface temperatures as shown in detail in Fig. 2. All in-depth sensors were mounted into a 2.54 cm diam cylindrical PICA core (Fig. 2a) that was subsequently inserted into the larger PICA model. The thermocouple probes were constructed of type S thermocouple wire of 0.127 mm diam encased in a 0.508 mm diam platinum sheath and insulated with MgO powder to prevent electrical shorting to the sheath wall. These sheathed probes were bent at 1.27 cm from their tips at a 90° angle to provide a configuration that allowed insertion into the test material along a constant depth line assumed to be along an isotherm and normal to the heat flux on the front face of test material. Such a temperature-sensing configuration with the sensor wires or sheaths aligned along an isotherm and having a sheath length to diameter ratio of at least 25:1 (as in this case) minimizes measurement error due to conduction losses [7]. Temperature measurement errors for these in-depth installations are estimated to be within ±5% of measured values based on the study of [8] for similar installations.

Accurate placement of both the sheathed thermocouple probes and the wire thermocouples was assured by insertion into carefully drilled holes at the specified depths measured from the unablated front face of the models (see Fig. 2b.) This procedure used precision fixtures that minimized the usual errors associated with thermocouple installations and provided accuracies at least as good as that determined by post-installation x-ray measurements.

An insulative coating was applied to the bare wire thermocouples by dipping into boron nitride slurry and then drying before insertion into the models. It was noted, however, that this coating was unevenly removed when the wire was pulled through the models during insertion so that the wire was probably not electrically insulated from the PICA either in the initial virgin or in the charred state. Only temperature measurements using the sheathed thermocouple probes are reported in this paper.

Bondline temperatures were measured by thermocouples (type K) mounted within the RTV bondline between the rear face of PICA models and the AETB layer. Backface temperatures were sensed with thermocouples (type K) attached to the rear face of this AETB material. Two bondline thermocouples were used on each model for redundancy.

Surface temperature data were obtained using two different single-wavelength optical pyrometers as well as a dual-wavelength (two-color) optical pyrometer. The two-color pyrometer provided the most consistent data, and surface temperature measurements

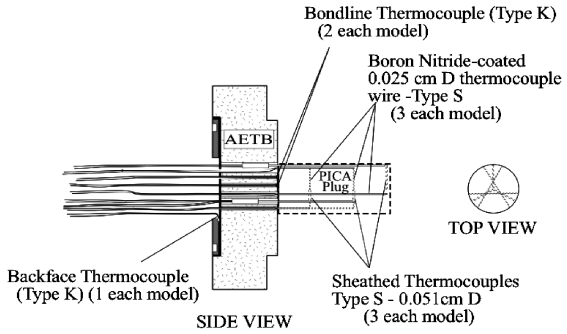

a) Thermocouple probes and bare wire thermocouple installation

Thermocouple In-Depth Locations
Distance from plug front face
(All dimensions in cm)

T/C	x	y	z	T/C to be used
1	0.20	-	-	Platinum sheath - Type S
2	-	1.60	-	Platinum sheath - Type S
3	-	-	3.60	Platinum sheath - Type S)
4	0.20	-	-	0.025 D bare wire BN-coated - Type S
5	-	1.60	-	0.025 D bare wire BN-coated - Type S
6	-	-	3.60	0.025 D bare wire BN-coated - Type S
7	In PICA/AETB bondline			Type K
8	In PICA/AETB bondline			Type K
9	In AETB/Al mounting plate bondline			Type K

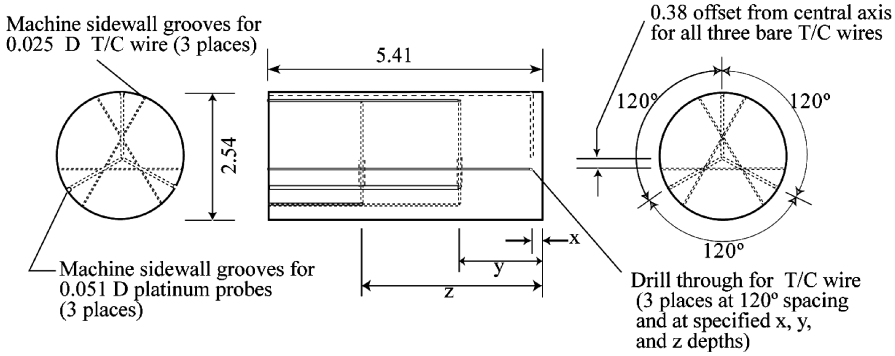

b) Typical Instrumented Plug

Fig. 2 Instrumentation details for 10.16 cm diam models.

reported herein are from this instrument. The estimated temperature error of the particular two-color pyrometer at 3315°C is estimated to be ±254°C for a 1% difference in ratio of emissivity at the two sensing wavelengths [9]. Based on emissivity data given in [2], PICA emissivity differences over these wavelengths are less than 1%. An imaging infrared video pyrometer system also was used to measure temporal temperature distributions on models during tests.

3. *Test Stream Calibrations*

Stream measurements were performed to set the heating rate and pressure conditions for these tests. For conditions used with the 2.54 and 5.08 cm diam models, two different hemisphere-cylinder copper heat sink calorimeters were used to measure the cold wall convective heating flux. One calorimeter had a diameter of 3.05 cm and a nose radius of 5.84 cm and the other had a diameter of 3.05 cm and a nose radius of 10.16 cm. Both calorimeters had a corner radius of 0.152 cm. The data from a series of calibration runs with these two calorimeters were used to select two test conditions. One selected condition gave a cold wall, fully catalytic heating rate of 1630 W/cm^2 for tests of the 2.54 cm diam models. This same condition provided a cold wall, fully catalytic convective heating rate of 1150 W/cm^2 for the 5.08 cm diam models. The measured stagnation pressure at this test condition for both smaller models was 0.65 atm. The actual measured values of these non-flat-faced calorimeters were corrected using the correlation factors of [10] to provide the assumed heating flux to the PICA models actually tested. The front surfaces of the copper heat sink mass in these calorimeters were carefully cleaned before each run to assure that a highly catalytic surface for dissociated gas species recombination was present to fulfill the assumption of a fully catalytic wall.

Calibration runs for the 10.16 cm diam models used 7.62 cm diam water-cooled hemisphere calorimeters with Gardon-type thin foil heat flux sensors mounted at the stagnation point to define two test conditions. One selected nominal condition for tests of the 10.16 cm diam PICA models was a cold wall, fully catalytic heating rate of 400 W/cm^2 and a stagnation point pressure of 0.20 atm, and the other was at a heating rate of 580 W/cm^2 and stagnation pressure of 0.45 atm. The relative calibration data variation for 10.16 cm diam calorimeters fell within a ±15% band with an estimated weighted error of approximately ±10% for the heating rate values at both stream conditions.

4. *Test Environments*

The arc jet test conditions and test times are shown in Table 1 for the 2.54 and 5.08 cm diam models and in Table 2 for the 10.16 cm diam models. The exposure times for these models varied from 4 to 38 s and resultant total heat loads were from 6.5 to 40.2 kJ/cm^2 (see Table 1). For the 10.16 cm diam models, the two different arc jet operating conditions provided model exposure times from 10 to 86 s, and total heat loads from 5.8 to 49.9 kJ/cm^2 on PICA models of varying thickness as shown in Table 2. The arc jet operating

conditions for all the tests was at a nominal stream total enthalpy of 29.5 MJ/kg. Radiation heating to the models from the shock layer at all of these conditions was negligible.

C. Material Performance Modeling

Modeling of the ablation and thermal performance of the PICA material used the FIAT (fully implicit ablation and thermal) computer code described in [11]. This code was used in a mode that models in-depth conduction, kinetically controlled pyrolysis, boundary layer blowing due to pyrolysis gases, and thermochemical surface recession as a function of time in a one-dimensional porous ablative material. The PICA properties used with this code were a combination of measured thermophysical properties and polymer pyrolysis kinetics, and adjusted property values based on thermal response data from these tests. The measured specific heat and thermal conductivity of virgin material were taken from [12]. The initial values from [12] for char thermal conductivity were iteratively adjusted to give the best fit to thermal response data over the range of test results. The Arrhenius kinetic constants for phenolic pyrolysis from [13] were used. The thermochemical and thermophysical properties resulting from this modeling process are given in the Appendix. It must be cautioned that these values for PICA char are derived from the specific modeling tool used (i.e., FIAT code) to match the data given in this paper, and cannot be assumed to be the true properties. These data may not give comparable or accurate results when used in other ablation response codes. Pyrolysis gas enthalpy values for the ablation products, and surface recession tables considering heterogeneous equilibrium among surface species, pyrolysis gas and boundary layer gaseous species were calculated using an equilibrium thermochemistry program [14]. A PICA char surface emissivity of 0.9 is consistent with the value [2] measured for PICA, and has been widely used for other carbonaceous ablators as supported by numerous sets of data. The PICA material ablation model was validated using the arc jet surface recession and thermal response data from these tests as discussed in following sections.

III. Data Analysis and Computational Model Comparisons

A. Ablation Performance

The 2.54 and 5.08 cm diam models were used at the highest heating rates and stagnation pressures, as previously described, to measure surface ablation rates at conditions approximating those for a nominal Stardust entry (1200 W/cm^2) and at least a 25% higher heating rate. The surface recession rate was taken as the best measure of ablative performance in this study. The recession rate data for these two smaller models are listed in Table 3, and recession rate data for the 10.16 cm models are given in Table 4. These data are plotted and compared in Figs. 3 and 4 to steady state surface recession rates calculated by the FIAT code for two different assumptions for the ablation condition. One condition assumed that the models respond as a one-dimensional, infinite slab material with all pyrolysis gases

Table 3 2.54 and 5.08 cm diam model recession data (IHF 121-I test series)

Model diameter, cm	Model no.	Run no.	Heating rate, W/cm^2	Max. surface temperature, °C	Heating time, s	Model thickness pretest, cm	Model thickness post-test, cm	Total recession, cm	Recession rate, cm/s
2.54	22	12W	1630	3078	8	5.72	4.96	0.76	9.49E − 02
2.54	23	12E	1630	1075	13	5.72	4.46	1.26	9.67E − 02
2.54	24	14W	1630	3099	8	5.72	3.92	0.72	9.05E − 02
2.54	26	14E	1630	3181	18	5.72	4.99	1.79	9.95E − 02
2.54	27	15W	1630	2945	4	5.72	4.44	0.42	1.04E − 01
2.54	28	15E	1630	2975	13	5.72	5.30	1.28	9.81E − 02
2.54	29	16W	1630	3212	15	5.72	4.27	1.45	9.65E − 02
2.54	30	16E	1630	3088	20	5.72	3.73	1.99	9.94E − 02
5.08	10	9E	1150	3068	30	5.66	5.02	1.13	4.04E − 02
5.08	11	9W	1150	3006	20	5.66	5.02	0.64	3.56E − 02
5.08	12	10E	1150	2626	35	5.66	4.32	1.35	4.08E − 02
5.08	13	10W	1150	2431	25	5.66	4.80	0.86	3.76E − 02
5.08	15	11E	1150	3181	40	5.66	4.00	1.66	4.38E − 02
5.08	14	11W	1150	3171	20	5.66	5.01	0.65	3.63E − 02
5.08	17	17E	1150	3191	30	5.66	4.55	1.11	3.98E − 02
5.08	16	17W	1150	3253	37	5.66	4.21	1.45	4.15E − 02

Table 4 10.16 cm diam model recession data (IHF 121-II test series)

Model no.	Run no.	Heating rate, W/cm^2	Heating time, s	Max. surface temperature, °C	Assembled model thickness: Pretest thickness, cm	Assembled model thickness: Post-test at center, cm	Assembled model thickness: Post-test at 2.54 cm radius, cm	Assembled model thickness: Post-test at corner, cm	Total recession at center, cm	Recession rate at center, cm/s
1	15E	580	69	2480	8.93	7.71	7.66	7.37	1.22	1.77E − 02
2	15W	580	86	2560	8.92	7.46	7.29	7.06	1.46	1.70E − 02
3A	14E	580	20	2719	5.11	4.76	4.74	4.66	0.35	1.73E − 02
3B	13E	580	40	2753	6.13	5.39	5.40	5.28	0.74	1.84E − 02
4B	13W	580	20	2749	6.13	5.80	5.75	5.69	0.33	1.66E − 02
6A	14W	580	20	2761	5.10	4.69	4.72	4.66	0.40	2.02E − 02
7A	12E	580	15	2441	5.60	5.33	5.33	5.27	0.27	1.81E − 02
7B	12W	580	15	2406	5.60	5.33	5.34	5.28	0.27	1.78E − 02
8A	11E	580	10	2618	5.63	5.47	5.43	5.38	0.16	1.63E − 02
8B	11W	580	20	2653	5.60	5.23	5.25	5.16	0.37	1.85E − 02
4A	17E	400	30	2417	5.10	4.78	4.74	4.65	0.32	1.08E − 02
5A	17W	400	30	894	5.12	4.75	4.75	4.65	0.37	1.24E − 02
5B	18E	400	40	2218	6.13	5.70	5.64	5.54	0.42	1.06E − 02
6B	18W	400	60	2496	6.13	5.43	5.40	5.28	0.70	1.17E − 02
9A	16E	400	15	2471	5.59	5.46	5.43	5.38	0.13	8.81E − 03
9B	16W	400	29	2489	5.61	5.26	5.26	5.18	0.35	1.20E − 02

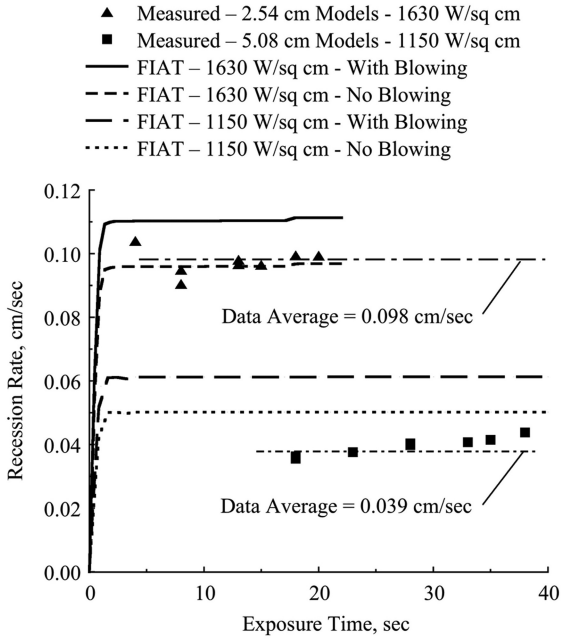

Fig. 3 Surface recession for 2.54 and 5.08 cm PICA models.

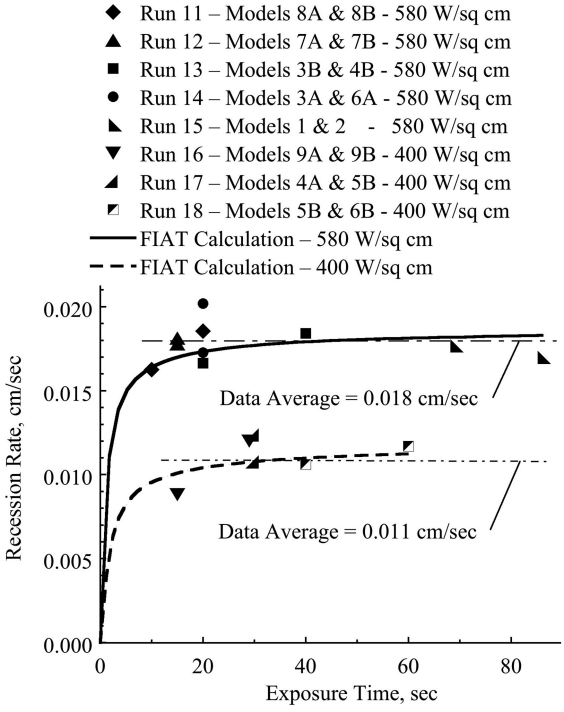

Fig. 4 Surface recession for 10.16 cm models.

escaping through the front surface and providing the maximum amount of boundary layer blowing. The other condition assumed that the polymer pyrolysis gases escaped out the sides of the models rather than through the front face with no front surface blowing, and that the surface recession was the result of only diffusion-controlled oxidation of the carbon surface. The data shown in Fig. 3 for 2.54 cm diam models and 5.08 cm diam models are much more closely matched by the assumption of no front surface blowing and with recession the result of oxidation only. The data in Fig. 3 show that the average measured recession rates of the smaller models are 12% lower at 1630 W/cm^2 and 36% lower at 1150 W/cm^2 than the steady state rate predicted for the case of one-dimensional, full surface blowing of ablation products, but are within 1% of the measured recession rate at 1630 W/cm^2 and are 22% lower than the predicted rate at 1150 W/cm^2 for the case assuming only diffusion-controlled oxidation with no blowing. It is clear that an assumption of no blowing/oxidation-only gives much better agreement with experiment, and this case is reasonable considering a combination of factors.

The better agreement of the case of diffusion-controlled oxidation-only calculation with the measured recession rate on the small models is consistent with several post-test observations. It was noted that a large fraction of phenolic polymer had been pyrolyzed from all parts of the models, leaving mostly a carbon matrix. This can be attributed to the high sidewall heating fluxes that clearly invalidate the assumption of one-dimensional, infinite slab heating inherent in the FIAT calculation model. Also, the small diameter of the models provides a smaller pressure drop, lower flow resistance path for pyrolysis gases to flow out of the sidewalls rather than the front surface. This also is inconsistent with the FIAT model which assumes one-dimensional heating and ablation.

The slight trend of increased recession rate with increasing heating times seen in the data may be explained by the observed progressive rounding of the model front face with increasing exposure time. Such rounding results in a decrease in the effective nose radius causing increased convective heating rate and an increase in recession rate. Also, an additional effect on ablation performance may be that the actual cold wall heating rates were different than those determined by stream calibrations, although the results for the two heating rate levels are not consistent with such a conclusion. An uncertainty of $\pm 10\%$ or greater in heating flux at these levels is certainly within operational experience with high-energy arc jets.

The data for surface recession of 10.16 cm models and comparison with the transient recession rate as calculated by the FIAT code assuming all pyrolysis gases escaped through the model front surface are given in Fig. 4. The plot shows that the average measured recession rates for both the 400 and 580 W/cm^2 levels agree very well with predictions from the FIAT code with the predicted steady state rate being about 2% higher at the 400 W/cm^2 level and about 1% higher at the 580 W/cm^2 condition. This excellent agreement between measured and predicted recession rates at these lower heating levels infers that assumptions of the FIAT calculation of a one dimensional infinite slab are better fulfilled for these larger diameter models. The predicted recession rate from the FIAT analytical model is satisfactory considering the range of high heating fluxes the model is applied to and the test and modeling parameter uncertainties. It is of interest to note that the curves for the calculated FIAT response show that, even at the 400–600 W/cm^2 heating range, there is a initial period of nonsteady ablation of 30 s or longer until steady state values of surface recession and temperature are reached.

Recession asymmetries were observed on the 2.54 and 5.08 cm models that are thought to be due to misalignment with the peak heating profile in the arc heater stream at the high heating rate conditions. Recession measurements were made only at the center for these models. Asymmetric recession was not observed on the 10.16 cm diam models, and recession measurements were made at the center, 1.0 cm away from the center, and at the edge of the model. The results are shown in Table 4. The front surface roughness on all models tested was greater post-test than on the pretest machined surfaces; however, the surfaces exhibited no evidence of large scale spallation and visually appeared reasonably smooth and uniform at all conditions.

B. Thermal Performance

Surface and in-depth temperature measurements from the 10.16 cm diam models were used to define the thermal response and to derive the analytical response model as previously discussed. The temperature data from a selected number of tests on these models were used to revise the thermophysical properties for use in the FIAT response code. None of the recession data from either the 2.54, 5.08, or 10.16 cm models were used for defining the properties because changes in these properties over ranges of interest have minimal effect on the recession rates. The data used were those from models 3B, 4B, 5B, 6A, 6B, 7B, and 9B, and these were selected because they were the most complete sets of data, had the best

instrumentation signal reliability, and included a representative range of PICA layer thicknesses from 2.23 to 3.25 cm and model diameter to thickness ratios from 4.55 to 3.125. The approach used to revise the modeling parameters was to modify only the char conductivity as previously discussed, and rerun the FIAT code for a new set of predictions that were compared with the experimental in-depth temperature profiles for the 7 sets of data from the models selected. This process was then iteratively repeated until it was judged that the revised model predictions were in reasonable agreement with the sets of measured data. The char thermal conductivity was chosen as the variable because it is the property with the greatest uncertainty.

Figures 5–10 show representative in-depth and surface temperature data and compare these data with FIAT code predictions using the revised property set that gave the best agreement. In general, the comparison of the agreement is based on maximum temperature reached at a given in-depth location because of an observed temperature rise lag that did not match the predicted monatomic temperature rise of the computer calculations. This failure to predict the observed lag in in-depth and bondline temperatures was found in data for this and other tests of PICA material, and is discussed more fully later in the paper. The maximum temperature was chosen for this reason as the basis of comparison between measured and predicted results. For each of the temperature plots of Figs. 5–10, the

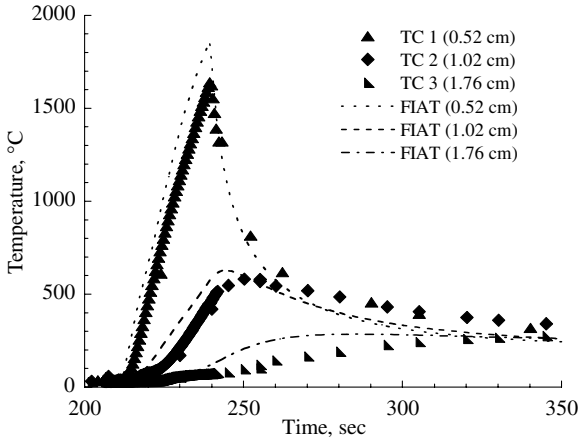

a) In-depth temperatures

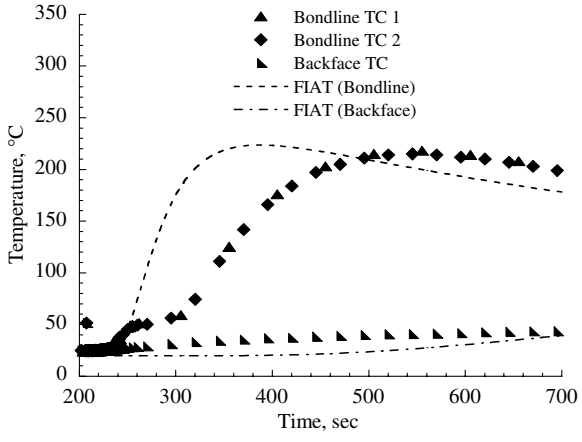

b) Bondline and backface temperatures

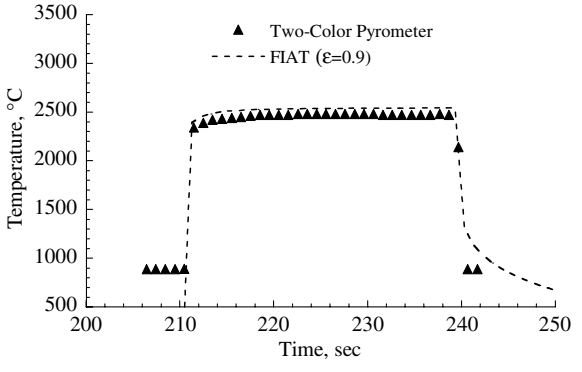

c) Surface temperature

Fig. 5 Comparison of experimental and calculated thermal response for model 9B. Heating rate = 400 W/cm^2; stagnation pressure= 0.20 atm; heating time 29 s.

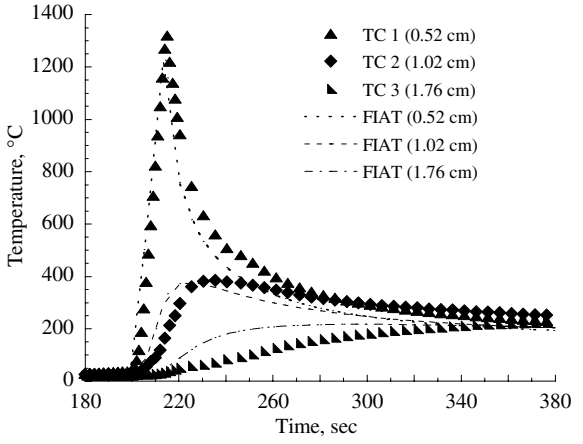

a) In-depth temperatures

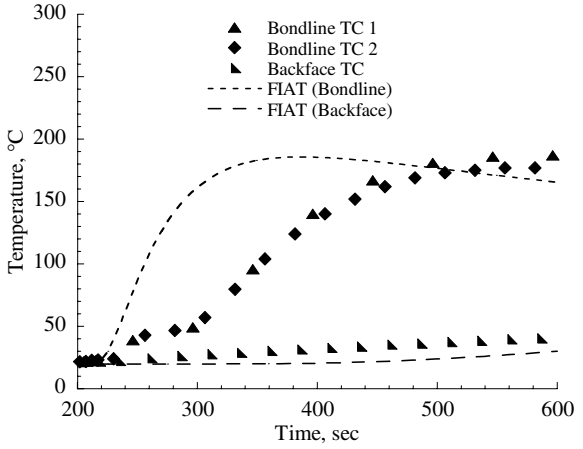

b) Bondline and backface temperatures

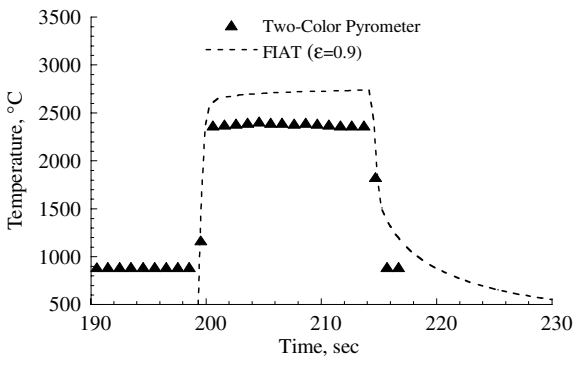

c) Surface temperature

Fig. 6 Comparison of experimental and calculated thermal response for model 7B. Heating rate = 580 W/cm^2; stagnation pressure= 0.45 atm; heating time = 15 s.

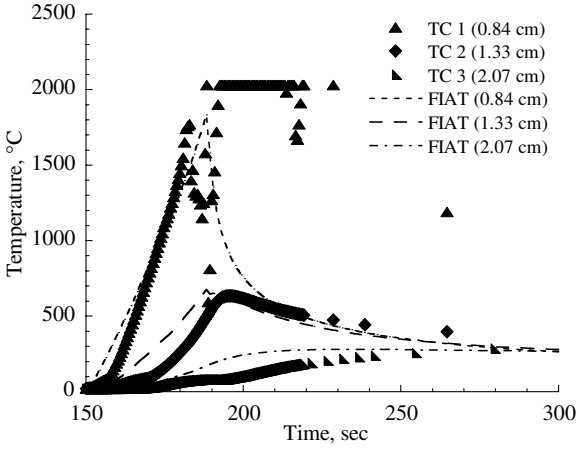

a) In-depth temperatures

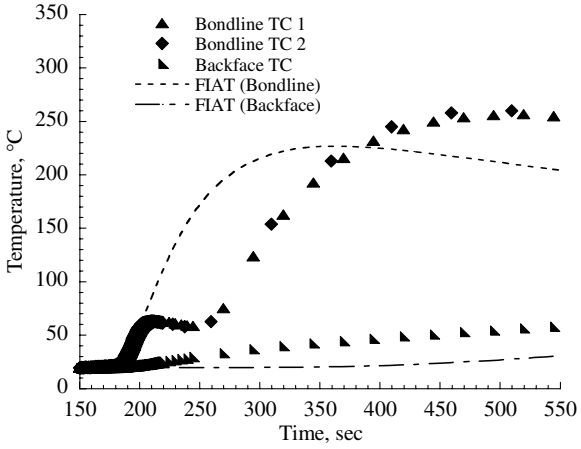

b) Bondline and backface temperatures

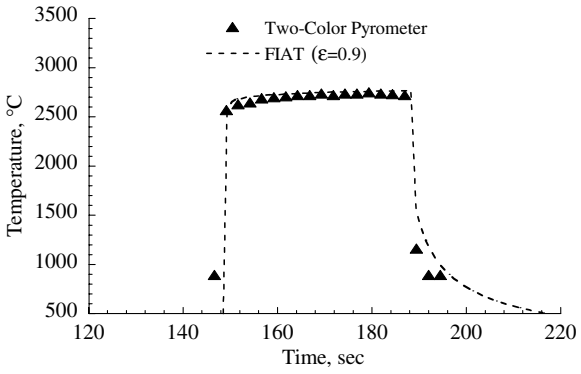

c) Surface temperature

Fig. 7 Comparison of experimental and calculated thermal response for model 3B. Heating rate = 580 W/cm^2; stagnation pressure= 0.45 atm; heating time = 40 s.

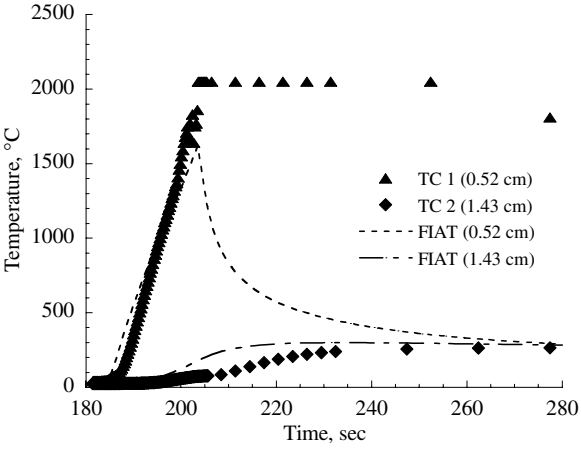

a) In-depth temperatures

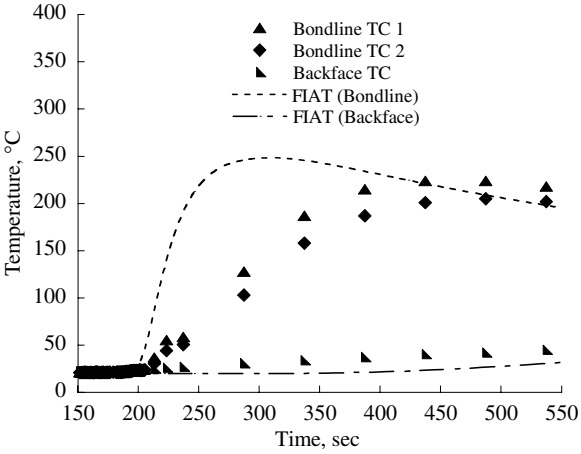

b) Bondline and backface temperatures

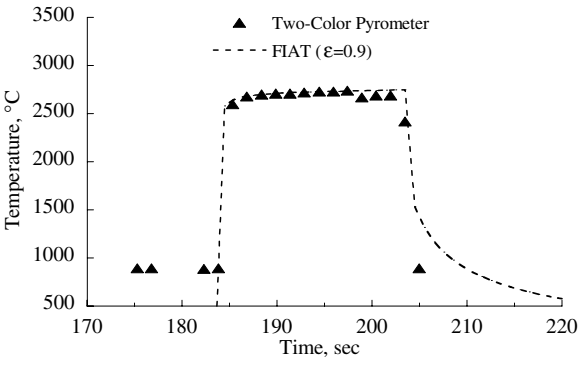

c) Surface temperature

Fig. 8 Comparison of experimental and calculated thermal response for model 6A. Heating rate = 580 W/cm^2; stagnation pressure= 0.45 atm; heating time = 20 s.

legends show in parentheses the depth of the installed thermocouple probes from the original unablated surface.

The data from model 9B are typical for the lowest heating rate of 400 W/cm^2. Model 9B had a test time of 29 s and an integrated heat load of 11.6 kJ/cm^2. In-depth thermocouple and pyrometer-measured surface temperature data are presented in Figs. 5a–5c for this model. It is seen that temperatures calculated with the FIAT code are in reasonably good agreement with the experimental data except for a mismatch in the prediction for the thermocouple closest to the surface (0.52 cm deep), a faster temperature rise than measured for this depth, and a failure to predict the bondline temperature response lag as shown in Fig. 5b.

Figures 6a–6c present a comparison of predicted in-depth, bondline, and backface temperatures from the FIAT code with experimental measurements for model 7B at a heating rate of 580 W/cm^2. In this case, the code predicts well the response of the thermocouple nearest the surface (0.52 cm deep), the peak in-depth temperatures at 1.016 and 1.755 cm depth, and the maximum bondline and backface temperatures. The measured surface temperature is about 300°C lower than the calculated level but is unaccountably lower than other pyrometer-measured temperatures at this same heating condition (cf., Fig. 7c). Again, the calculated response does not accurately simulate the lag in temperature rise at the 1.016 and 1.755 cm deep locations or at the bondline. The data

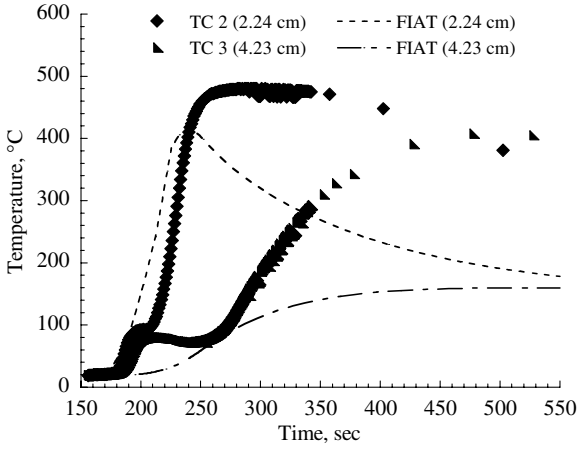

a) In-depth temperatures

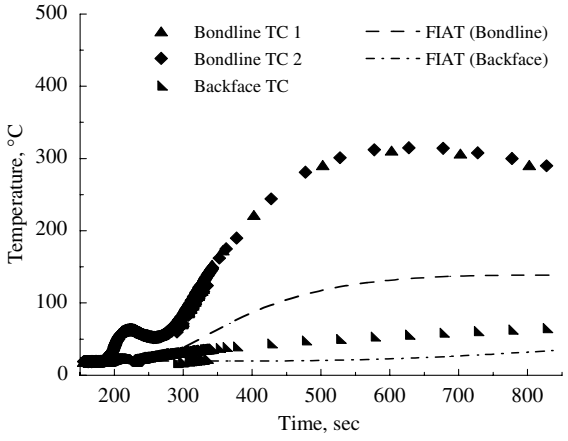

b) Bondline and backface temperatures

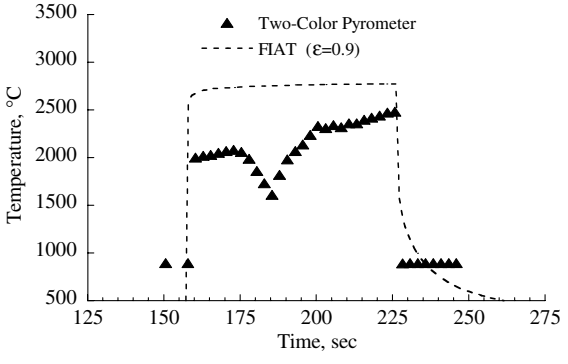

c) Surface temperature

Fig. 9 Comparison of experimental and calculated thermal response for model 1. Heating rate = 580 W/cm^2; stagnation pressure= 0.45 atm; heating time = 69 s.

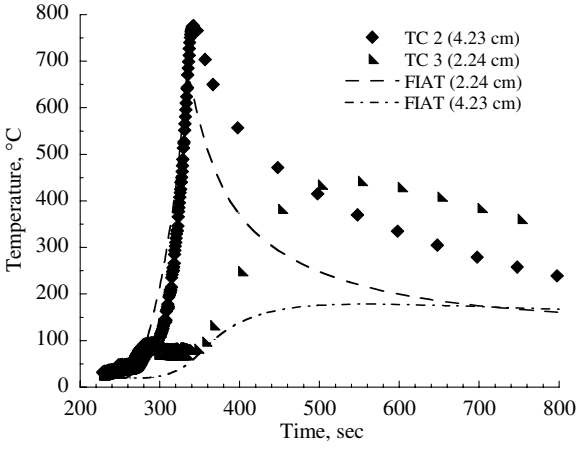

a) In-depth temperatures

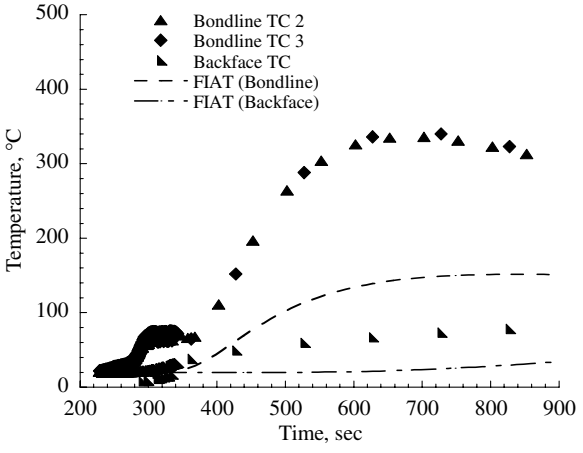

b) Bondline and backface temperatures

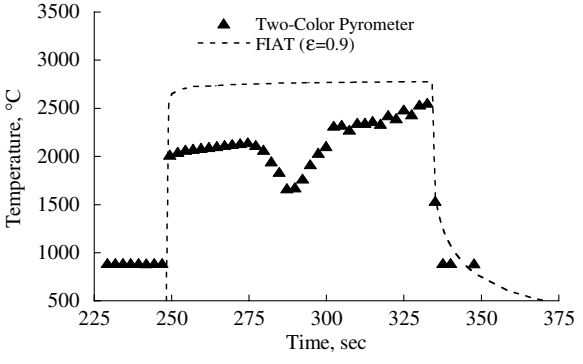

c) Surface temperature

Fig. 10 Comparison of experimental and calculated thermal response for model 2. Heating rate = 580 W/cm^2; stagnation pressure= 0.45 atm; heating time = 86 s.

from the test of model 3B show similar results in Figs. 7a–7c. For this model, Fig. 7a shows that the thermocouple probe melted at about the temperature expected for platinum (1769°C). The FIAT calculation is seen to predict well the maximum temperatures measured at 1.334 and 2.073 cm depths, and the maximum of the two bondline temperatures, but the calculated response did not match the lag in the measured temperature rise seen in Figs. 7a and 7b. The calculated and experimental surface temperatures are seen to be in excellent agreement in this case for the entire test time (Fig. 7c). Another example presented for results at a heating level of 580 W/cm^2 is given in Figs. 8a–8c for model 6A. This is the thinnest 10.16 cm diam model tested with a pretest thickness of 2.23 cm. The thermocouple probe closest to the surface (0.52 cm deep) melted at a temperature consistent with the melting point for platinum (Fig. 8a) as would be expected. The other response of the other in-depth thermocouple (1.43 cm deep) is matched by the computer prediction for maximum temperature (Fig. 8b). The calculated and measured surface temperatures are seen to agree well.

Figures 9 and 10 show results for models 1 and 2 that were tested at a heating rate of 580 W/cm^2 for the longest test times and highest integrated heat load of all the 10.16 cm models. Model 1 was exposed for 69 s with a resulting heat load of 40.0 kJ/cm^2, and model 2 was heated for 86 s for a total heat load of 49.9 kJ/cm^2. Both of these two tests exceeded the total heat load value (36 kJ/cm^2) expected for the Stardust SRC entry with the nominal entry trajectory but were somewhat less than the expected heat load of 55 kJ/cm^2 for an overshoot trajectory entry. These two models were the thickest tested with 6.04 cm of PICA backed by the 2.54 cm thick AETB layer. In

both models 1 and 2, data for thermocouple probes closest to the surface (0.89 cm deep) indicated failure from melting within the first 20 s of exposure with a response very similar to that shown for model 3B in Fig. 7a. This initial response was reasonably predicted by the FIAT calculation (cf., Fig. 7a) and corresponding plots for models 1 and 2 are not included. The other in-depth thermocouple data for model 1 are presented in Fig. 9a, and indicate that temperatures at 2.24 and 4.23 cm were considerably higher than predicted by FIAT calculations. This same discrepancy is seen in Fig. 9b for the bondline and backface temperatures. Measured maximum surface temperature is seen to be more than 200°C lower than the FIAT code prediction, but this is attributed to pyrometer misalignment because other tests at this same heating condition show much higher temperatures that agree with the FIAT prediction. The same response for model 2 can be seen in Figs. 10a–10c. Again the computer model results badly underpredict the in-depth, bondline, and backface measured temperatures in contrast to the much better agreement on thinner PICA models. The best explanation for this FIAT underprediction is that the assumption of one-dimensional ablation and heat conduction inherent in the FIAT model is not valid on these thick models with a large sidewall area exposed to high heating levels. This conclusion is also supported by temperature rise differences between the computer predictions and the measured values. The more rapid onset of the measured in-depth temperature rise seen in Figs. 9a, 9b, 10a, and 10b is consistent with heat being conducted inward from sidewall heating. A post-test cross-section photo (Fig. 11) of one of these models after being cut into two halves clearly shows that considerable degradation had progressed from the model sides toward the center, thus invalidating the assumption of one-dimensional heat transfer.

The measured in-depth temperatures characterized by an expected increase with time followed by a leveling off at temperatures between 50 to 100°C to a constant or, in some cases, a decreasing temperature value (cf., Figs. 5b, 6b, 7b, 8b, 9a, 9b, 10a, and 10b) has been observed in other heating tests of PICA and similar phenolic impregnated materials. For example, this same feature is evident in temperature data from arc jet tests during PICA development [12]. Similar features are seen in data from other heating tests of materials with phenolic resin impregnation dating back to at least 1968 but apparently have not been documented. An unidentified endothermic process within the PICA material can explain this behavior. Phase transition processes are known to show similar effects on transient temperature data in other materials. It is clear that the FIAT code with the material properties and ablation chemical kinetics used for this study did not capture this behavior. The resolution of this modeling inconsistency is the subject of a further study to be published later.

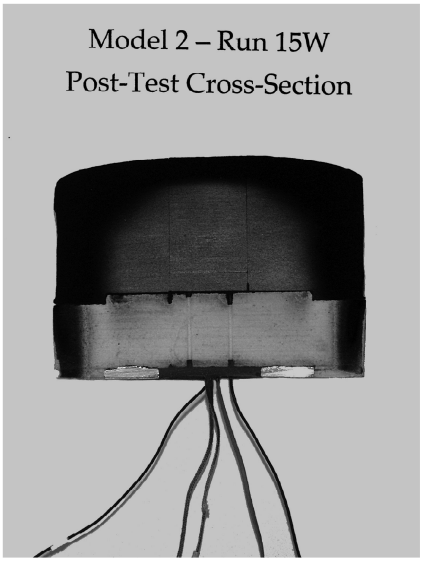

Fig. 11 Post-test photo of model 2 cross section that shows internal ablation resulting from sidewall heating.

C. Application to Stardust Flight Heat Shield Design

An objective of this investigation was to verify the Stardust SRC forebody heat shield design for Earth reentry. The major design criterion for this vehicle heat shield was a maximum allowable bondline temperature of 250°C. The revised PICA properties derived from iterative adjustment to provide best fits to data shown herein were used with the FIAT computer code to recalculate the surface recession, maximum temperatures, and design margins. Figures 12 and 13 present the results of this newer calculation and a comparison to the original design. In Fig. 12, the calculated bondline temperature as a function of spacecraft entry time is plotted for both the baseline design trajectory heating rate (1200 W/cm^2) and for a 25% increase in heating rate (1500 W/cm^2). The result from the original calculation using the baseline Stardust properties also is shown. It is seen that the calculated maximum bondline temperatures for the

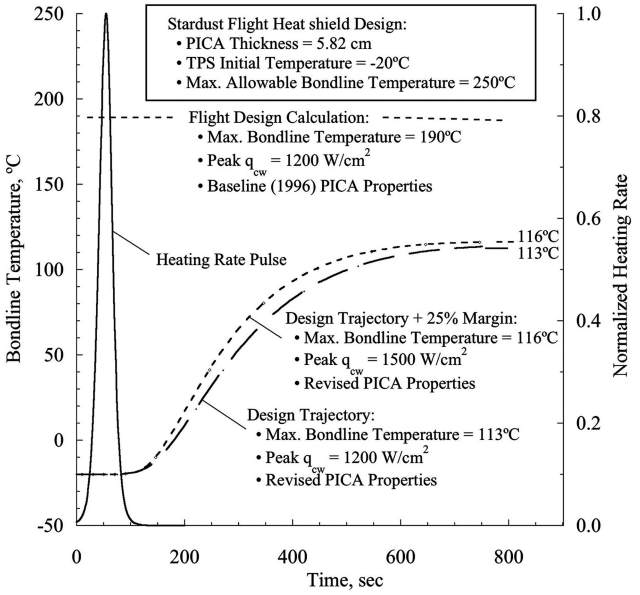

Fig. 12 Comparison of calculated bondline temperatures for Stardust heat shield design using baseline properties and using revised model properties.

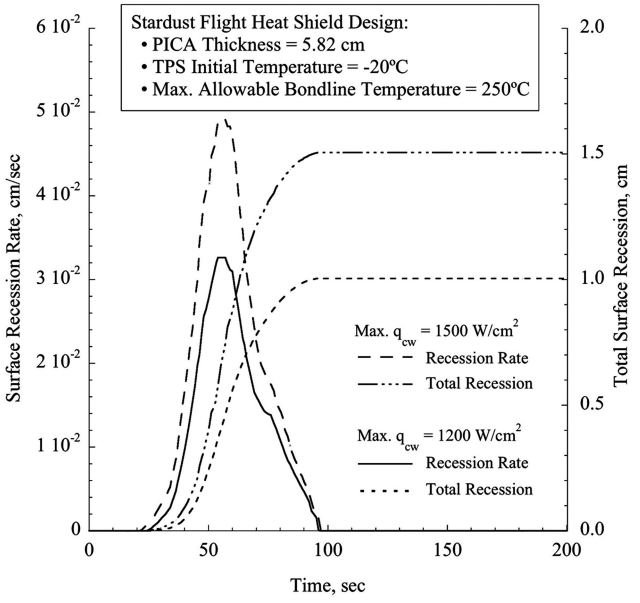

Fig. 13 Comparison of calculated surface recession rate and total recession for Stardust heat shield design using baseline properties and using revised model properties.

cases of nominal design heating and of a 25% added margin are all well below the design maximum allowable temperature of 250°C. The recalculated maximum temperature of about 115°C is also less than that from the earlier calculation result with baseline properties of 190°C. The calculated surface recession rates for the revised PICA properties are shown in Fig. 13 for both the nominal design case of 1200 W/cm^2 and the increased margin case of 1500 W/cm^2. The higher heating rate entry would result in a 50% increase in total recession (1 cm vs 1.5 cm) but would still be a fraction of the total as-designed heat shield thickness of 5.82 cm. The calculated maximum recession rates shown in Fig. 12 of up to about 0.05 cm/s for nominal entry heating conditions are less than those experimentally measured rates in this study, thus giving added confidence in the use of PICA material for the Stardust heat shield design.

IV. Summary and Conclusions

Extensive arc jet tests at conditions simulating the design Earth entry heating conditions for the Stardust sample return capsule were conducted as part of this investigation to evaluate the heat shield design. The resulting data on ablative surface recession and internal temperature response were used to iteratively modify thermophysical properties for PICA material used in the FIAT computer code to satisfactorily predict the experiment response using surface recession rate and maximum internal temperatures as criteria. An apparent endothermic process at low temperatures during PICA ablation resulted in a delayed internal temperature rise that was not captured by computer code results using either the baseline or the revised properties. A separate study is underway to investigate this previously undocumented process. The predictive results using the FIAT code, however, did agree with measured surface recession and maximum internal temperature data so that the use of this code with the revised property set can predict with good confidence the performance of the actual Stardust heat shield design. It was concluded that the results of this study have validated the original Stardust PICA forebody heat shield design, and provided evidence for lower than previously predicted maximum temperatures at the adhesive bondline attaching the shield to the spacecraft structure. These results increase confidence in the heat shield design for the Stardust sample return capsule.

Appendix: Thermophysical properties for PICA

Thermophysical properties for PICA are shown in Tables A1 and A2. A note of caution is needed for these data. The PICA char thermal conductivity and char specific heat values were derived by a process of matching FIAT model predictions with experimental arc jet data on PICA response. Therefore, the use of these data with other modeling software or computational methods may not give valid results for PICA performance prediction. These data should not be considered to be independent of the FIAT code used for their derivation.

Table A1 Virgin material properties; density = 0.266 g/cm^3

Temperature, K	Specific heat, kJ/kg–K	Thermal conductivity, W/cm–K	Emissivity
256	0.879	3.97E − 04	0.80
294	0.984	4.02E − 04	0.80
444	1.298	4.16E − 04	0.80
556	1.465	4.53E − 04	0.80
644	1.570	4.70E − 04	0.80
833	1.716	4.86E − 04	0.80
1111	1.863	5.23E − 04	0.80
1389	1.934	5.60E − 04	0.80
1667	1.980	6.98E − 04	0.80
1944	1.988	8.72E − 04	0.80
2222	2.001	1.11E − 03	0.80
2778	2.009	1.75E − 03	0.80
3333	2.009	2.78E − 03	0.80

Table A2 Char material properties; density = 0.210 g/cm^3

Temperature, K	Specific heat, kJ/kg–K	Thermal conductivity, W/cm–K	Emissivity
256	0.733	3.97E − 04	0.90
294	0.783	4.02E − 04	0.90
444	1.093	4.16E − 04	0.90
556	1.319	4.53E − 04	0.90
644	1.432	4.70E − 04	0.90
833	1.674	4.86E − 04	0.90
1111	1.842	5.23E − 04	0.90
1389	1.967	5.60E − 04	0.90
1667	2.051	6.05E − 04	0.90
1944	2.093	7.29E − 04	0.90
2222	2.110	9.22E − 04	0.90
2778	2.135	1.46E − 03	0.90
3333	2.152	2.32E − 03	0.90

Acknowledgments

This work was supported by NASA Ames Research Center under Contract NAS2-99092 with Eloret Corporation. The assistance of William Willcockson of the Lockheed Martin Company in providing data and material is gratefully acknowledged. The authors would like to thank James Arnold and Ethiraj Venkatapathy of NASA Ames for continued support and their valuable comments and suggestions.

References

[1] Vellinga, J., Craig, C. L., Gellis, R. T., Rasbach, C. E., Rogers, J. J., Thorton, M. G., Willcockson, W. H., Brownlee, D. E., and Atkins, K. L., "Environmental Design Considerations for Stardust," Society of Automotive Engineers, Paper 972278, July 1997.

[2] Tran, H., Johnson, C. E., Rasky, D. J., Hui, F. C., Hsu, M.-T., Chen, T., Chen, Y.-K., Paragas, D., and Kobayashi, L., "Phenolic Impregnated Carbon Ablators (PICA) as Thermal Protection Systems for Discovery Missions," NASA TM-110440, April 1997.

[3] Tran, H., Johnson, C., Hsu, M-T., Smith, M., Dill, H., Chen-Jonsonn, A., "Qualification of the Forebody Heatshield of the Stardust's Sample Return Capsule," AIAA Paper 97-2482, June 1997.

[4] Winovich, W., and Carlson, W., "The 60-MW Shuttle Interaction Heating Facility," *Proceedings of the 25th International Instrumentation Symposium*, Instrument Society of America, Pittsburgh, PA, 1979, pp. 59–75.

[5] Olynick, D., Chen, Y. K., and Tauber, M., "Forebody TPS Sizing with Radiation and Ablation for the Stardust Sample Return Capsule," AIAA Paper 97-2474, June 1997.

[6] Zoby, E. V., "Empirical Stagnation-Point Heat Transfer Relation in Several Gas Mixtures at High Enthalpy Levels," NASA TN D-4799, June 1968.

[7] "Standard Practice for Internal Temperature Measurements in Low-Conductivity Materials," ASTM Standard E-377, Dec. 1996.

[8] Baker, D. L., Wool, M. R., and Shaeffer, J. W., "Development of Total and Radiative Heat Flux Measurement Systems for Rocket Nozzle Applications," Aerotherm Corporation, Final Report No. 70-11, Mt. View, CA, Aug. 1970.

[9] Anon., "*M190 User's Manual (Appendix B)*," Mikron Infrared, Inc., Oakland, NJ, May 1995.

[10] Zoby, E. V., and Sullivan, E. M.,"Effects of Corner Radius on Stagnation-Point Velocity Gradients on Blunt Axisymmetric Bodies," NASA TN X-1067, March 1965.

[11] Chen, Y.-K., and Milos, F. S., "Ablation and Thermal Response Program for Spacecraft Heatshield Analysis," AIAA Paper 98-0273, Jan. 1998.

[12] Anon., "Final Report on Thermal Properties of Lightweight Charring Ablators," Fiber Materials, Inc., FMI EMTL Final Report No. 1648, Biddeford, ME, July 1994.

[13] Goldstein, H. E., "Pyrolysis Kinetics of Nylon 6-6, Phenolic Resin, and Their Composites," *Journal of Macromolecular Science, Part A*, Vol. 3, No. 4, 1969, pp. 649–673.

[14] "User's Manual, Aerotherm Chemical Equilibrium Computer Program, (ACE81)," Acurex Corporation, Report UM-81-11/ATD, Mt. View, CA, Aug. 1981.

T. Lin
Associate Editor